Proceedings World Geothermal Congress 2015
Melbourne, Australia, 19-25 April 2015

Modelling of Productivity Decline in Geothermal Reservoirs due to Fines Migration-Induced Formation Damage

Zhenjiang You[1], Alexander Badalyan[1], Yulong Yang[1], Pavel Bedrikovetsky[1], Martin Hand[2], Chris Matthews[2]

[1]Australian School of Petroleum, The University of Adelaide, Adelaide, South Australia, 5005, Australia

[2]Institute of Minerals and Energy Resources, The University of Adelaide, Adelaide, South Australia, 5005, Australia

zhenjiang.you@adelaide.edu.au

Keywords: geothermal well; fines migration; formation damage; mathematical model; productivity decline; temperature effect

ABSTRACT

Production history of geothermal well A (Australia) indicates fines migration as a primary mechanism of productivity decline. A new method to determine movable fines and consequent permeability decline from fragments has been developed. Both fragments and cores are available from the analogous Ladbroke formation. Good agreement between the movable fines concentration from Ladbroke fragments and cores validates the developed method. The method has been applied to well A fragments for productivity decline prediction.

Mobilised fines concentrations and permeability damage from rock fragments and cores data for Ladbroke formation validates the method. Good agreement between the laboratory-based mathematical modelling of fines migration in well A with the field data is observed, resulting in identification of fines migration and clogging as the formation damage mechanism. The sensitivity study shows that geothermal reservoirs are significantly more vulnerable for permeability damage by fines mobilisation than conventional oil and gas fields, since the particle attaching forces are weaker at elevated temperatures.

Fines migration is recognised as a frequent cause for permeability damage and well productivity decline in conventional oil and gas wells. A mathematical model successfully predicts formation damage of studied geothermal reservoir due to fines migration and straining. This model can be used for skin prevention, mitigation and removal.

The laboratory-based mathematical modelling of productivity decline in well A allows for long-term prediction of well index, for calculation of the minimum flow rate preventing fines mobilisation and for recommendations on damage mitigation.

1. INTRODUCTION

Although the productivity decline during operative life of geothermal wells has been observed and investigated intensively, only phenomenological analysis of productivity decline is available on a purely empirical basis (Aragón-Aguilar, Barragán-Reyes et al. 2013). The mechanisms leading to the productivity impairment in geothermal reservoirs and the recommendations on possible damage mitigation have not yet been thoroughly studied.

Fines migration induced formation damage and permeability reduction in porous media has been widely reported in the literature for geothermal reservoirs (Priisholm, Nielsen et al. 1987; Baudracco 1990; Rosenbrand, Haugwitz et al. 2014). The phenomenon is explained by fine particle mobilisation, where the mechanical equilibrium of attaching electrostatic force and detaching drag and lifting forces is disturbed at high velocity or reduced salinity; the lifted particles are strained in thin pores causing the permeability reduction (Bedrikovetsky, Siqueira et al. 2011). Reduced values of electrostatic forces attaching fines to grain surfaces at high temperatures suggest the geothermal well clogging to be higher than that in oil and gas wells. However, the productivity impairment due to fines migration in geothermal reservoirs has not been investigated so far.

The classical mathematical model for colloidal suspension flow in porous media assumes that the particle detachment rate is proportional to the differences between the current and critical values of parameters, i.e. velocity, salinity, pH, temperature, etc., where the critical values of parameters correspond to the beginning of detachment (Bradford, Kim et al. 2009; Gitis, Rubinstein et al. 2010). This model exhibits asymptotic stabilisation after abrupt change of the parameters, while the laboratory tests show an instant response to the abrupt parameter change (Ochi and Vernoux 1998). The model contains empirical proportionality coefficients that can be obtained only from tuning the laboratory data and does not account for mechanical equilibrium. The modified particle detachment model uses the maximum concentration of attached particles as a function of velocity, salinity, pH, temperature, etc., instead of the kinetic expression for the detachment rate in the classical model (Bedrikovetsky, Siqueira et al. 2011). The modified model is free of the above mentioned shortcomings of the classical model. Therefore, in the current work the maximum retention function is used to describe fine particle detachment during the exploitation of geothermal wells.

Maximum retention function of velocity is determined from laboratory tests with increasing velocity (Ochi and Vernoux 1998; Badalyan, Carageorgos et al. 2014). Limited range of flow rates provided by the available pumps restricts experimental measurement of the maximum retention function versus velocity. In the present work, taking advantage of both salinity and velocity dependencies of the maximum retention function as solutions to the particle torque balance equation, a new method of translating the salinity dependency of the maximum retention concentration into the velocity dependency is proposed. It allows evaluation of the maximum retention function versus velocity from salinity variation coreflood tests.

Maximum retention function and formation damage coefficient are determined by least square adjustment of coreflood data. However, cores are not always readily available. In the cases where cores are unavailable but rock fragments are available (e.g.,

geothermal well A, Australia), the proposed method of determining permeability and maximum retention function from rock fragments is highly valuable.

2. EXPERIMENTAL STUDY

This section briefly describes the materials used, laboratory setup and experimental procedure. More details on experimental work are provided elsewhere (Badalyan, Carageorgos et al. 2014).

2.1 Materials

Two sandstone cores LG-1/c (2553.25 m depth) and LG-2/c (2557.12 m depth) are 3.92 cm in diameter and 4.86 and 6.33 cm in lengths, respectively. Leftover pieces of rock are crushed to fragments LG-1/f and LG-2/f. Fragments from S-1 well S-1/f (2903-2906 m) are available. Cores and fragments are evacuated at the residual vacuum of 1.5 Pa for 24 hours. Then, they are saturated with 0.6 M NaCl solution prepared from the degassed deionised MilliQ water to prevent particles in cores and fragments from mobilisation. Rock samples have the following porosities: 18.2 % (LG-1/c and LG-1/f), 17.2 % (LG-2/c and LG-2/f) and 10.6 % (S-1/f).

2.2 Experimental setup and procedure

The laboratory setup applied in the current work is schematically shown in (Badalyan, Carageorgos et al. 2014). The experimental procedure includes the following steps: study of the effect of alternating fluid velocities on particle mobilisation and permeability for cores and composite porous media made of spherical borosilicate glass beads and fragments; measurements of particle concentrations in outlet streams; calculation of retained particle concentration as a function of fluid velocity; collection of particles mobilised and passed through porous media and their SEM-EDAX analyses for identification of minerals; and calculation of DLVO total potential energy of interaction between porous matrix and particles at various experimental conditions. This method determines conditions favourable to particle mobilisation, fines removal capacity of cores and fragments, and their effect on formation damage.

2.3 Permeability evaluation using composite porous media

In the case that core samples are unavailable but rock fragments are available, a new experimental method is proposed for evaluation of rock permeability from composite porous media. In the test of LG-1/f fragment samples, the following parameters are measured for a glass beads-only-formed porous medium: length of the column l_b = 5.089×10^{-2} m, radius of the column r_b = 1.213×10^{-2} m, and permeability k_b = 1148 mD. Measured permeability of a non-damaged LG-1/c sample is k_f = 28.326 mD, and is adopted as permeability for a non-damaged LG-1/f sample. Volumes of glass beads and fragments are measured. Assume they fill the entire cross-section of a thick-walled stainless steel cylinder. The equivalent lengths for glass beads and fragments are equal to l_b^{eq} = 4.067×10^{-2} m and l_f^{eq} = 1.022×10^{-2} m, respectively. Permeability of rock fragments is calculated as:

$$k_f = \frac{l_f^{eq}\alpha}{\frac{l_{comp}}{k_{comp}} - \frac{l_b^{eq}}{k_b}} \tag{1}$$

in which l_{comp} = 5.089×10^{-2} m is the length of a composite porous medium; k_{comp} is the permeability of a composite porous medium; α is a fitting parameter. Applying experimental data k_f for LG-1/c sample to Eq. (1) yields α = 4.27×10^{-2}. Permeability for a non-damaged rock fragment sample k_f = 10.12 mD is obtained from (1). Permeability for S-1/f sample varies from 2.9 to 6.9 mD according to the well completion report (PANAX-Geothermal 2010), and decreases from 10.5 to 5.58 mD with increase of fluid velocity according to lin-log method presented in petro-physics report. The agreement between the present result and those from the two reports is satisfactory. A good match is observed between measured permeability for LG-1/c and LG-2/c samples and fragment permeability evaluated using the proposed method (Figure 1).

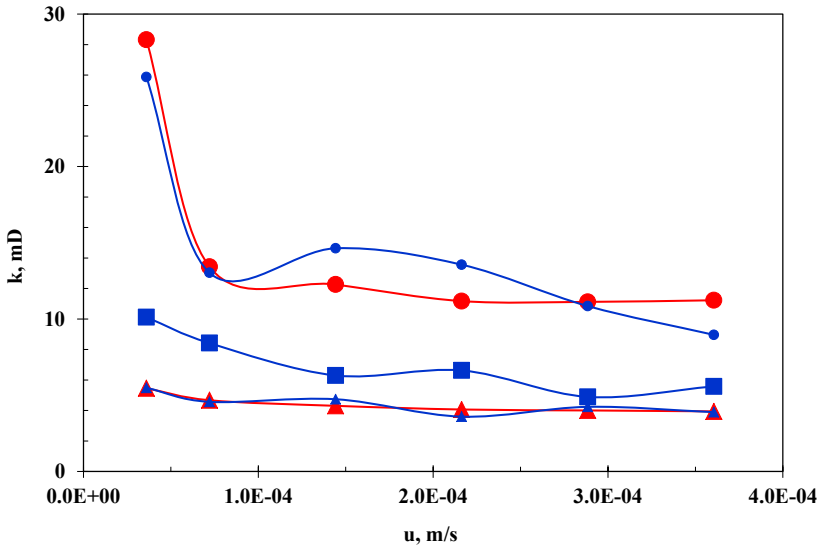

Figure 1: Effect of fluid velocity on rock permeability.

2.4 SEM-EDAX analyses on released fines

SEM-EDAX analyses results for fines released from LG-1/f sample are presented in Figure 2. Typical kaolinite booklets are visible in SEM image (see Figure 2a). EDAX spectrum for this booklet (see Figure 2b) exhibits typical ratio of aluminum-to-silicon atomic distributions as approximately 1:1 according to the general chemical formula for kaolinite clay $Al_2Si_2O_5(OH)_4$. All elements typical for chlorite according to the general formula $(Mg,Al,Fe)_{12}[(Si,Al)_8O_{20}](OH)_{16}$ are presented in EDAX spectrum for flakes (see Figure 2c) indicating to chlorite morphology.

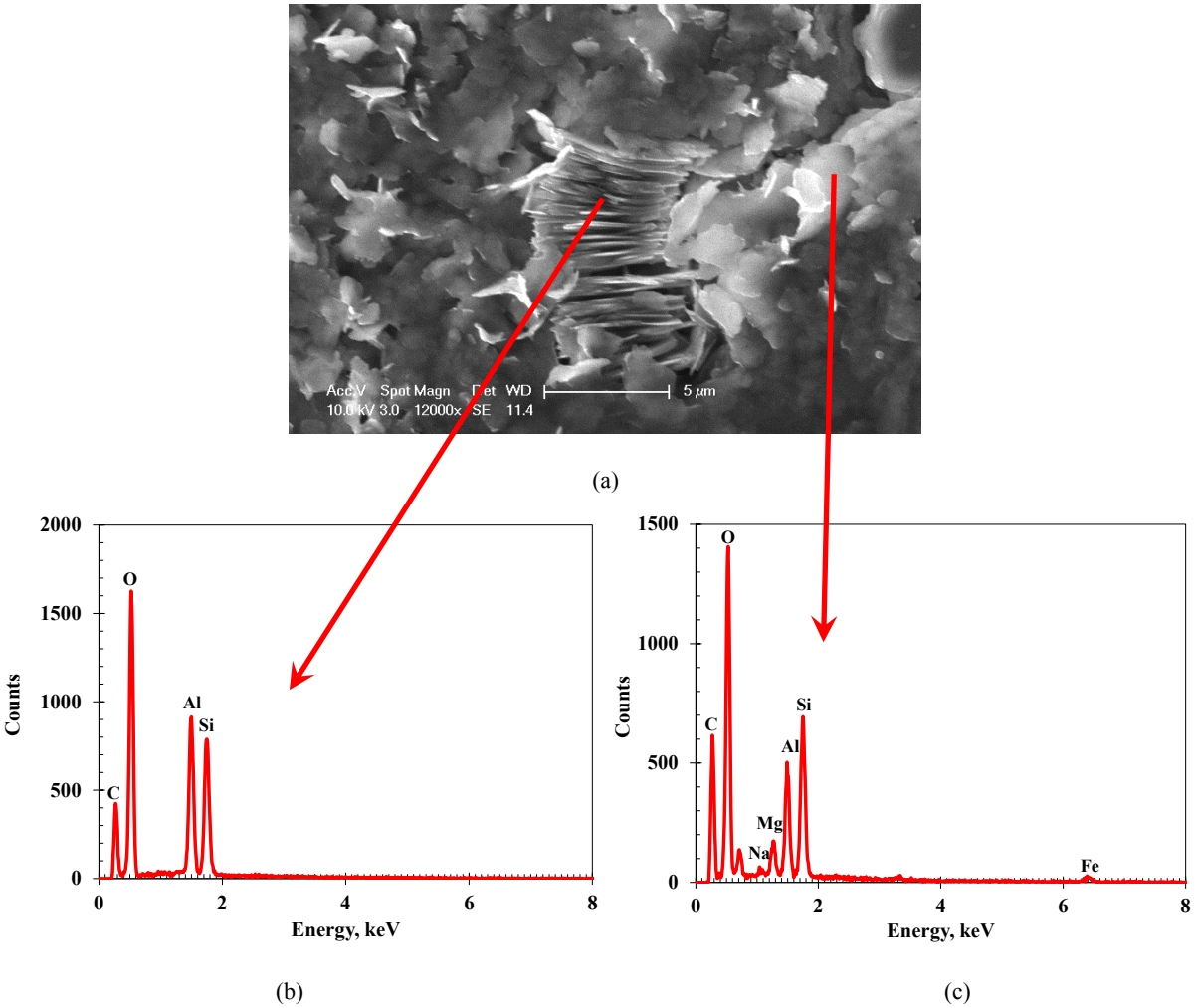

Figure 2: SEM image (a) and EDAX spectra for kaolinite (b) and chlorite (c) for LG-1/f sample.

3. FINES MOBILISATION CHARACTERISATION USING SALINITY SENSITIVITY

3.1 Maximum retention concentration

Fine particles on the rock surface are subject to the following forces: electrostatic force F_e, drag force F_d, lifting force F_l and gravitational force F_g. The drag and lifting forces detach the particle from the grain surface while the electrostatic and gravitational forces attach it. It is assumed that at the moment of leaving the solid surface, the particle rotates around the neighbouring attached particles or around a spike of the surface. Therefore, the condition of mechanical equilibrium of a fine particle on the rock surface is the net zero of the total torque exerting on the particle (Freitas and Sharma 2001; Bedrikovetsky, Siqueira et al. 2011).

In general, the concentration of attached particles is a function of the ratio between the detaching and attaching torques ε (Bedrikovetsky, Siqueira et al. 2011):

$$F_d(U,r_s)l(r_s) = F_e(\gamma,r_s) - F_l(U,r_s) + F_g(r_s), \quad l = l_d / l_n \tag{2}$$

$$\sigma_a = \sigma_{cr}(\varepsilon) \tag{3}$$

$$\varepsilon = \frac{F_l(U)+l_d l_n^{-1} F_d(U)}{F_e+F_g} \tag{4}$$

where ε is the erosion ratio and the dependency (3) is called the maximum retention function. Eqs. (3, 4) also describe the dependency of the maximum attached concentration versus pH, temperature and the concentrations of different ions.

3.2 Using salinity sensitivity to characterise fines mobilisation

The inflow performance in geothermal production well are considered. The flow velocity U varies by two orders of magnitude depending on the distance from the well. Therefore, the main dependence that characterises fines mobilisation is $\sigma = \sigma_{cr}(U)$. However, changing flow rate in laboratory in such a wide range is difficult. For example, significant increase in flow rate in the available range of rates 15-20 L/s for commercially available pumps involves inertial non-linear effects which are subject to future research.

Nevertheless, change of salinity γ is an available option in the laboratory. Both salinity and velocity dependencies of the maximum retention function are solutions to the torque balance equation (2). It allows translating the salinity dependency of the maximum retention concentration $\sigma_{cr}(\gamma)$ into the velocity dependency $\sigma_{cr}(U)$, and vice versa. The translation is given by the following equation

$$\sigma_{cr} = \left[1 - \left(\frac{\mu r_s^2 U}{\phi H F_e(\gamma_0) x(\gamma_0)}\right)^2\right](1-\phi_c)\phi = \left[1 - \left(\frac{\mu r_s^2 U_0}{\phi H F_e(\gamma) x(\gamma)}\right)^2\right](1-\phi_c)\phi \qquad (5)$$

where $x = \frac{\mu r_s^2 U}{\phi H(1-2h/H)F_e}$ is the ratio between the drag and electrostatic forces.

The coreflood test with piecewise decreasing salinity was performed in the laboratory (Badalyan, Carageorgos et al. 2014). Measured permeability history and accumulative particle concentration at the outlet are shown in Figure 3 and Figure 4, respectively. Mathematical model for fines migration in porous media (detailed derivations are provided in the Appendix) are applied to treat the experimental data by optimisation. Results from modelling show good agreement with the measured data for both permeability (Figure 3) and outlet concentration (Figure 4). The optimised values of model parameters are: initial retention concentration σ_{a0}=4.45×10^{-4}, mean particle size r_s=0.79 μm, coefficient of variance for particle size distribution C_v=0.64 μm. Formation damage coefficient β, filtration coefficient λ and drift delay factor α in each stage of piecewise constant salinity are listed in **Error! Reference source not found.**.

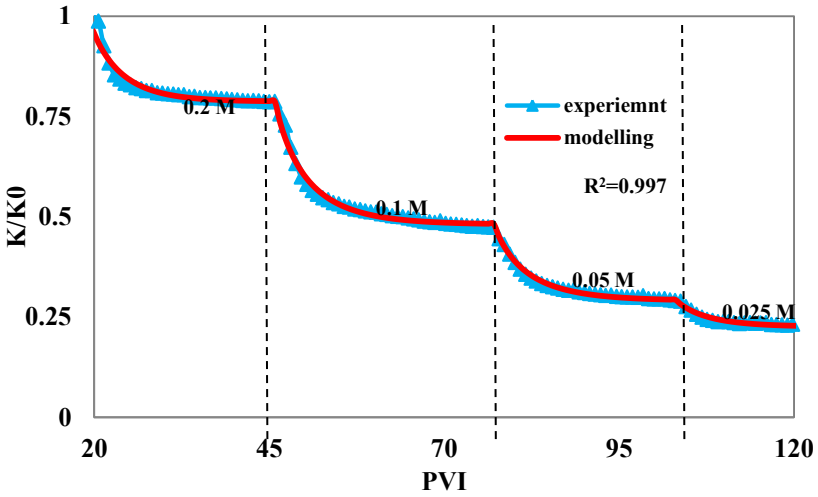

Figure 3: Permeability decline history during coreflood with piecewise decreasing salinity (experimental and modelling results).

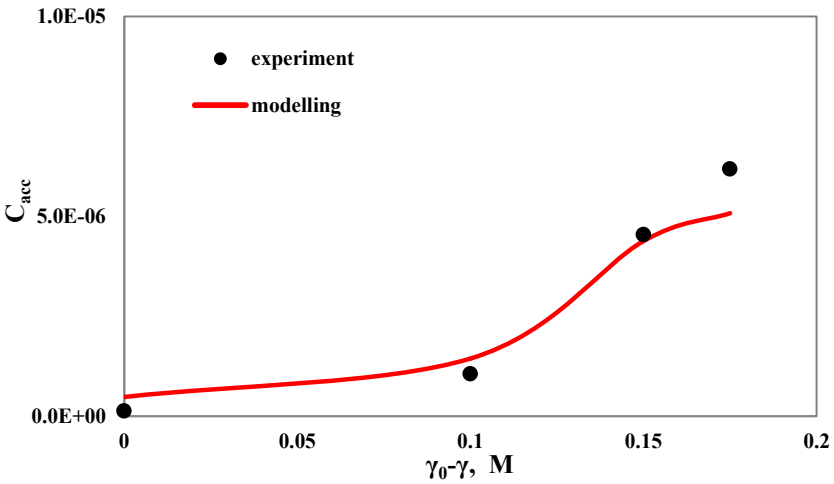

Figure 4: Accumulative outlet concentrations at different salinities (experimental and modelling results).

Table 1: Optimised values of model parameters.

β_1	β_2	β_3	β_4
7032.3	9470.7	5549.0	12154
λ_1	λ_2	λ_3	λ_4
79.93	70.56	40.46	37.51
α_1	α_2	α_3	α_4
0.00250	0.00224	0.00359	0.00476

The salinity dependency of σ_{cr} calculated from laboratory data based modelling is presented in Figure 5(a). Translation to the velocity dependency of σ_{cr} using Eq. (5) yields the profile shown in Figure 5(b), which will be applied to field case study in next section.

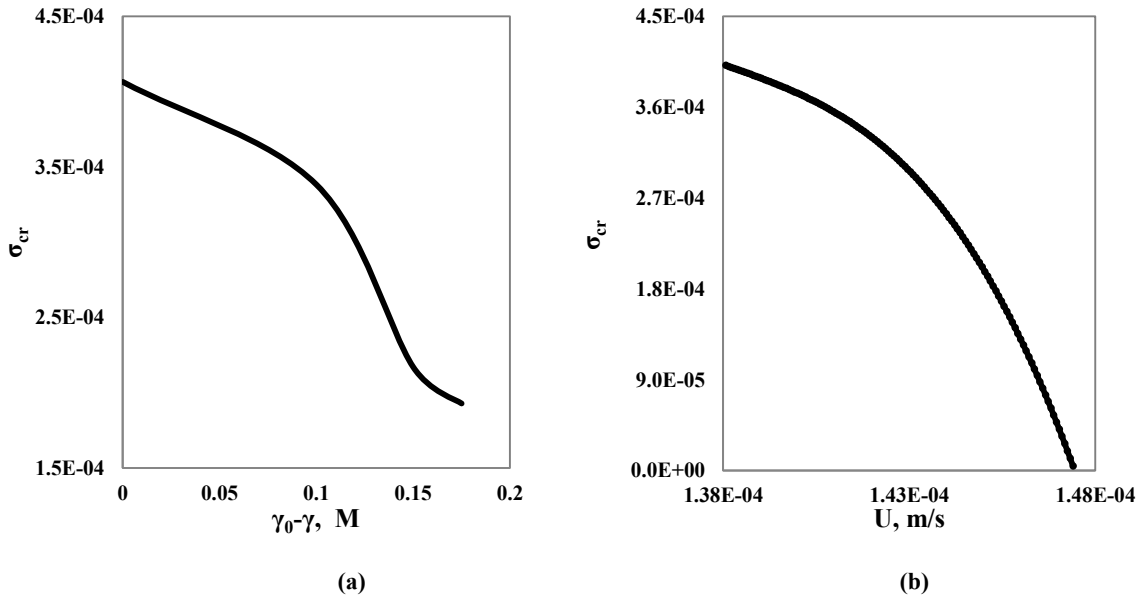

Figure 5: Maximum retention concentration: (a) salinity dependency; (b) velocity dependency.

4. PRODUCTIVITY DECLINE – FIELD CASE STUDY

A mathematical model for flow towards wellbore accounting for fines migration induced formation damage (You, Badalyan et al. 2014) was applied to geothermal well A (Australia) for field case analysis. The well was discharged for 5 hours with a rate range of 15-25 L/s. Pressure drawdown was increased from 20 bars at the beginning of discharge up to 55 bars at the end. The normalised reciprocal of well index (so called the impedance J)

$$J(t) = \Delta p(t)q(0)/\Delta p(0)q(t) \tag{6}$$

gradually increased during the discharge and tended to an asymptotic value at later times. The impedance increase is attributed to the permeability decline in wellbore neighborhood due to straining of the mobilised fine particles. Star points in Figure 6 correspond to field data, while the continuous curve is generated from the modelling results. Good agreement between the well data and the mathematical modelling results is observed (the coefficient of determination R^2 = 0.98), which validates the mathematical model.

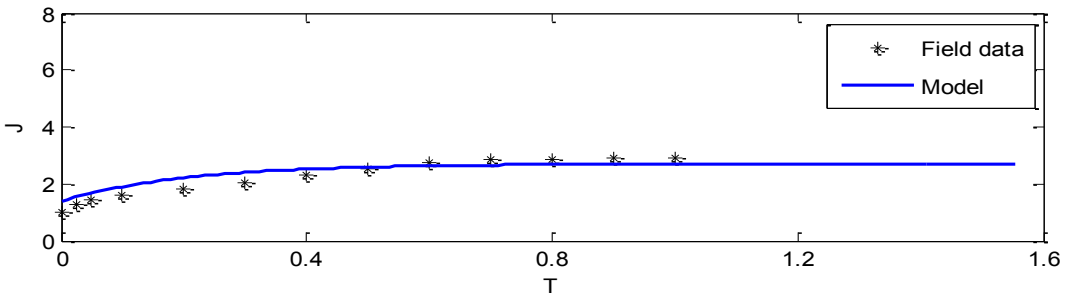

Figure 6: Well impedance growth during well exploitation.

The results of sensitivity study with respect to reservoir temperature are shown in Figure 7. The continuous curve correspond to the conditions of geothermal field A, with reservoir temperature $T_2 = 129$ °C. Other values of temperature are: $T_1 = 100$ °C, $T_3 =$

200 °C and $T_4 = 300$ °C. The higher is the temperature, the lower is the maximum retention concentration of attached fines, and the larger is the amount of mobilised particles. Therefore, the well impairment increases as reservoir temperature increases (Figure 7).

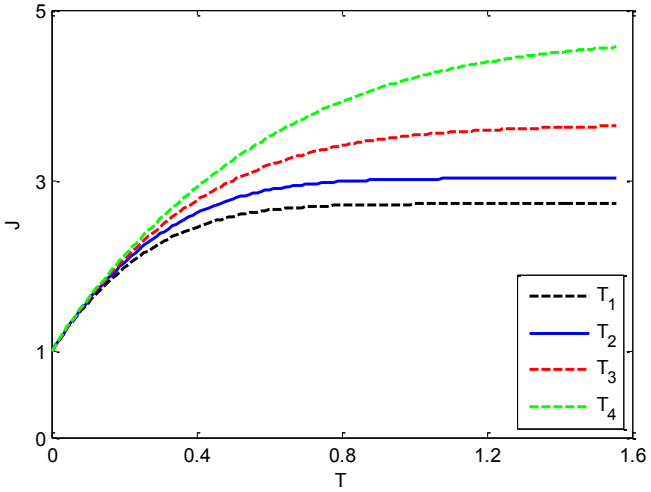

Figure 7: Effect of temperature on the well impedance profile.

5. CONCLUSIONS

- Estimation of well formation damage was carried out by evaluation of fines removal capacity and fines migration in rock fragments instead of cores. The proposed method correlates permeability for cores and fragments very well.
- Both salinity and velocity dependencies of the maximum retention function are solutions to the particle torque balance equation, which allows translation between the salinity and the velocity dependencies of the maximum retention concentration for attached particles.
- Well productivity history in field A (Australia) and the modelling-based prediction are in a good agreement.
- Elevated temperatures leads to lower maximum retention concentration and higher well impedance.

ACKNOWLEDGEMENTS

The authors acknowledge the Department for Manufacturing, Innovation, Trade, Resources and Energy (DMITRE), the Plan for Accelerating Exploration (PACE) scheme, the Australian Renewable Energy Agency (ARENA), and the South Australian Centre for Geothermal Energy Research (SACGER) for providing research support.

REFERENCES

Aragón-Aguilar, A., R. M. Barragán-Reyes and V. M. Arellano-Gómez (2013). "Methodologies for analysis of productivity decline: A review and application." Geothermics **48**: 69-79.

Badalyan, A., T. Carageorgos, Z. You, U. Schacht, P. Bedrikovetsky, C. Matthews and M. Hand (2014). A new experimental procedure for formation damage assessment in geothermal wells. Thirty-Ninth Workshop on Geothermal Reservoir Engineering, Stanford University, Stanford, California, AGEA.

Baudracco, J. (1990). "Variations in permeability and fine particle migrations in unconsolidated sandstones submitted to saline circulations." Geothermics **19**(2): 213-221.

Bedrikovetsky, P., F. D. Siqueira, C. A. Furtado and A. L. S. Souza (2011). "Modified Particle Detachment Model for Colloidal Transport in Porous Media." Transport in Porous Media **86**(2): 353-383.

Bradford, S. A., H. N. Kim, B. Z. Haznedaroglu, S. Torkzaban and S. L. Walker (2009). "Coupled factors influencing concentration-dependent colloid transport and retention in saturated porous media." Environmental Science and Technology **43**(18): 6996-7002.

Freitas, A. M. and M. M. Sharma (2001). "Detachment of particles from surfaces: An AFM study." Journal of Colloid and Interface Science **233**(1): 73-82.

Gitis, V., I. Rubinstein, M. Livshits and G. Ziskind (2010). "Deep-bed filtration model with multistage deposition kinetics." Chemical Engineering Journal **163**(1-2): 78-85.

Ochi, J. and J. F. Vernoux (1998). "Permeability decrease in sandstone reservoirs by fluid injection: Hydrodynamic and chemical effects." Journal of Hydrology **208**(3-4): 237-248.

PANAX-Geothermal (2010). Well testing program for Salamander-1. Sinclair Knight Merz: 112.

Priisholm, S., B. L. Nielsen and O. Haslund (1987). "Fines migration, blocking, and clay swelling of potential geothermal sandstone reservoirs, Denmark." SPE Formation Evaluation 2(2): 168-178.

Rosenbrand, E., C. Haugwitz, P. S. M. Jacobsen, C. Kjøller and I. L. Fabricius (2014). "The effect of hot water injection on sandstone permeability." Geothermics **50**: 155-166.

You, Z., A. Badalyan, P. Bedrikovetsky, M. Hand and C. Matthews (2014). "Productivity decline in Salamander geothermal well: experiment, modelling and case study." APPEA Journal **54**.

APPENDIX: MATHEMATICAL MODEL FOR FINES MIGRATION IN POROUS MEDIA

In this Appendix we present a detailed derivation of the mathematical model for suspension flow in porous media, accounting for slow migration of detached fines. The model is applied to the treatment of experimental data in Sec. 3.

The population balance equation takes into account of all the suspended, attached and strained fines in porous media:

$$\frac{\partial\left(\phi c+\sigma_s+\sigma_a\right)}{\partial t}+U\alpha\frac{\partial c}{\partial x}=0 \tag{A1}$$

Particle straining rate is proportional to the suspension flux:

$$\frac{\partial\sigma_s}{\partial t}=\lambda\left(\sigma_s\right)\alpha U c \tag{A2}$$

Darcy equation accounts for permeability decline due to particle straining:

$$U=-\frac{k_0}{\mu\left(1+\beta\sigma_s\right)}\frac{\partial p}{\partial x} \tag{A3}$$

The following constitutive equation describes attached particle concentration assuming instant release of movable fines:

$$\sigma_a\left(U\right)=\min\left(\sigma_{a0},\sigma_{a,\max}\left(U\right)\right) \tag{A4}$$

Thus, the suspended fines concentration due to particle release can be expressed as:

$$\Delta c=\phi^{-1}\left(\sigma_a\left(t_i\right)-\sigma_a\left(t_{i-1}\right)\right)=\phi^{-1}\Delta\sigma_a\left(U_{i-1},U_i\right) \tag{A5}$$

Initial and boundary conditions include:

$$\begin{aligned}&c\left(x,0\right)=0,\ \ c\left(0,t\right)=0\\&\sigma_a\left(x,0\right)=\sigma_{a0}\\&\sigma_s\left(x,0\right)=0\end{aligned} \tag{A6}$$

where c is suspended concentration, σ_a is attached concentration, σ_s is strained concentration, λ is filtration coefficient, β is formation damage coefficient, k_0 is initial permeability, μ is suspension viscosity, p is pressure.

Introduce the following dimensionless variables to the governing system (A1-A6):

$$S_a=\frac{\sigma_a}{\phi},S_s=\frac{\sigma_s}{\phi},\lambda_D=\lambda L,t_D=\frac{\int_0^t U\left(y\right)dy}{\phi L},x_D=\frac{x}{L},\alpha=\frac{U_s}{U} \tag{A7}$$

The dimensionless equations are obtained as:

$$\frac{\partial\left(c+S_s\right)}{\partial t_D}+\alpha_i\frac{\partial c}{\partial x_D}=0 \tag{A8}$$

$$\frac{\partial S_s}{\partial t_D}=\alpha_i\lambda_{Di}c \tag{A9}$$

$$S_a\left(x_D,t_D\right)=\min\left(S_{a0},S_{a,\max}\left(U_i\right)\right) \tag{A10}$$

$$c\left(x,t_{Di}\right)=c_{i-1}\left(x_D\right)+\Delta S_a\left(U_{i-1},U_i\right),\ c\left(0,t_D\right)=0 \tag{A11}$$

The permeability is calculated as:

$$k_i(t_D) = \frac{k_{i-1}}{1 + \beta\phi\int_0^1 S_{si}dx_D} = \frac{k_0}{\prod_{K=1}^{K=i}\left[1 + \beta_k\phi\int_0^1 S_{sk}[t_{D(k+1)}]dx_D\right]} \tag{A12}$$

where S_{si} is the net retention concentration at Stage i.

Suspended fines concentration is solved from (A8- A9) by the method of characteristics:

$$c = \begin{cases} 0, & x_D \le \alpha_i(t_D - t_{Di}) \\ \left[c_{i-1} + \Delta S_a(U_{i-1}, U_i)\right]e^{-\alpha_i\lambda_{Di}(t_D - t_{Di})}, & x_D > \alpha_i(t_D - t_{Di}) \end{cases} \tag{A13}$$

where $\alpha_i = dx_D/dt_D$ is the speed of propagation of the concentration front.

After defining

$$Q_i(t_D) = e^{-\alpha_i\lambda_{Di}(t_D - t_{Di})} \tag{A14}$$

suspended fines concentration in Stage i accounting for the particles inherited from previous stages is expressed as:

$$c_i(j) = \begin{cases} 0 & j = 1 \\ \sum_{j=2}^{j=i+1}\left(\Delta S_a(U_{i-j+1}, U_{i-j+2})\prod_{K=i-j+2}^{K=i} Q_K\right), & j > 1 \end{cases} \tag{A15}$$

The principle of mass balance indicates that the total retained concentration in porous media is equal to the initial suspended concentration minus the sum of the concentration of exiting particles and the concentration of particles moving in the core. Therefore, the retained concentration is obtained as:

$$\int_0^1 S_{si}(x_D, t_D)dx_D = \underbrace{\frac{\Delta\sigma_i}{\phi} + \int_0^1 c_{i-1}(x_D, t_{Di})dx_D}_{initial\ particles} - \left(\underbrace{\int_{t_{Di}}^{t_D}\alpha_i c_i(1, t_D)dt_D}_{exiting\ particles} + \underbrace{\int_0^1 c_i(x_D, t_D)dx_D}_{moving\ particles}\right) \tag{A16}$$

where

$$\int_0^1 c_{i-1}(x_D, t_{Di})dx_D = \sum_{j=2}^{j=(i-1)+1}\left(\left(\left[x_{D(i-1)}\right]_j - \left[x_{D(i-1)}\right]_{j-1}\right)\Delta S_a(U_{(i-1)-j+1}, U_{(i-1)-j+2})\prod_{K=(i-1)-j+2}^{K=i-1} Q_K\right) \tag{A17}$$

$$\int_{t_{Di}}^{t_D}\alpha_i c_i(1, t_D)dt_D = \frac{1}{\lambda_{Di}}\left[1 - \exp(-\alpha_i\lambda_{D_i}(t_D - t_{Di}))\right]\left(\Delta S_a(U_{i-2+1}, U_{i-2+2}) + \sum_{j=3}^{j=i+1}\left(\Delta S_a(U_{i-j+1}, U_{i-j+2})\prod_{K=i-j+2}^{K=i-1} Q_K\right)\right) \tag{A18}$$

$$\int_0^1 c_i(x_D, t_D)dx_D = \sum_{j=2}^{j=i+1}\left(\left(\left[x_{Di}\right]_j - \left[x_{Di}\right]_{j-1}\right)\Delta S_a(U_{i-j+1}, U_{i-j+2})\prod_{K=i-j+2}^{K=i} Q_K\right) \tag{A19}$$

Substituting the expressions for retained concentration (A16-A19) into (A12) results in the permeability at each stage.